A novel algorithm for solving multiplicative mixed-norm regularization problems

Mathieu Aucejo, Olivier de Smet

A novel algorithm for solving multiplicative mixed-norm regularization problems

M. Aucejo[a], O. De Smet[a]

[a]*Structural Mechanics and Coupled Systems Laboratory, Conservatoire National des Arts et Métiers, 2 Rue Conté, 75003 Paris, France*

Abstract

In a paper, recently published in *Mechanical Systems and Signal Processing*, a multiplicative mixed-norm regularization has been introduced for solving space-frequency force reconstruction problems. Originally, the solution is obtained from an Iteratively Reweighted Least-Squares (IRLS) algorithm. However, as shown in this communication, such an algorithm exhibits a lack of robustness regarding the measurement noise level. For this reason, a novel iterative resolution algorithm, based on the first-order optimality condition, is introduced. From a numerical experiment, it is shown that the proposed algorithm exhibits a better robustness than the IRLS algorithm initially implemented for solving force reconstruction problems in the frequency domain.

Keywords: Inverse problem, Force reconstruction, Multiplicative regularization, Mixed-norm regularization

*Corresponding author. E-mail address: mathieu.aucejo@lecnam.net

1. Introduction

Mixed-norm regularization are used in the inverse problems community to promote several features of a signal to recover[1] and introduce an explicit coupling its component. Such a regularization technique has been widely studied in signal and image recovery applications [1–9]. In the context of force reconstruction, Rezayat et al. first derive a mixed $\ell_{2,1}$-regularization to reconstruct broadband point forces [10, 11] from G-FISTA (Grouped Fast Iterative Shrinkage-Thresholding Algorithm). This particular mixed-norm regularization has then been applied by Wambacq et al. using an interior point method [12] and by Qiao et al. using an accelerated gradient descent method [13]. However, these particular forms of additive regularization are based on the assumption that the regularization parameter can be adequately selected. A proper choice of the regularization parameter is all the more crucial as it conditions the quality of the reconstructed solutions. In the abovementioned papers, the regularization parameter is either determined using expensive a posteriori procedure (i.e. computation of the solution for predefined values and choosing the best one) or manually tuned (with a non negligible risk of mistuning).

To circumvent the problems associated to the selection f the regularization parameter, we have recently proposed a multiplicative mixed-norm regularization for solving space-frequency force reconstruction problems based on a general $\ell_{p,q}$-regularization term [14]. Theoretically, the main advantage of such a regularization strategy is to simultaneously exploit one's prior knowl-

[1] The term signal has to be understood in a wide sense.

edge of the spatial distribution of the sources to identify (located/distributed) as well as any prior information about their frequency content (broadband /narrow-band). From the mathematical standpoint, the proposed space-frequency multiplicative regularization consists in defining the target excitation vector $\widehat{\mathbf{F}}$ as the solution of the following minimization problem:

$$\widehat{\mathbf{F}} = \underset{\mathbf{F}\setminus\{\mathbf{0}\}}{\operatorname{argmin}} \|\mathbf{X} - \mathbf{H}\mathbf{F}\|_2^2 \cdot \|\mathbf{F}\|_{p,q}^q, \tag{1}$$

where

- $\mathbf{X}$ is the global vibration vector, including the measured vibration fields for all the frequencies of interest. If n_m is the number of measurement points and n_f the number of frequencies considered, $\mathbf{X}$ has dimension $(n_m \cdot n_f) \times 1$;
- $\mathbf{F}$ is the global force vector, built by stacking the force vectors at each studied frequency. If n_r is the number of reconstruction points, $\mathbf{F}$ has dimension $(n_r \cdot n_f) \times 1$;
- $\mathbf{H}$ is the global transfer functions matrix. It is a block diagonal matrix including all the transfer functions matrices in the frequency range of interest. Considering the respective dimensions of $\mathbf{X}$ and $\mathbf{F}$, $\mathbf{H}$ has dimension $(n_m \cdot n_f) \times (n_r \cdot n_f)$.
- $\|\bullet\|_{p,q}$ is the mixed $\ell_{p,q}$-norm defining the space-frequency regularization term.

In the definition of the space-frequency regularization term, q is the tuning parameter describing one's prior knowledge of the spatial distribution of the

sources, while p is the tuning parameter related to prior information about the spectral content of the excitation sources. Practically, the value of p and q must be set so as to properly reflect available prior information. In this regard, $q \leq 1$ for promoting sparse sources, while $q \geq 2$ for distributed sources. In the same vein, $p \leq 1$ if the excitation signal is rather narrow band, while $p \geq 2$ if the excitation signal is supposed to be broadband. Although defining adapted values of p and q is far from obvious for non-experienced user, they can actually be wisely chosen from a careful analysis of the mechanical system under consideration.

In the original paper, the resolution of the space-frequency multiplicative regularization defined in Eq. (1) is performed through the implementation of an adapted Iteratively Reweighted Least-Squares algorithm [14–16]. However, it has recently been shown that, for force reconstruction problems, IRLS-like (a.k.a IRℓ_2) algorithm could be less robust than Iteratively Reweighted (IR) algorithm, built from the direct application of the first-order optimality condition, w.r.t. the measurement noise level [17].

In the light of these results, the aim of this paper is twofold: first derive a novel IR algorithm based on the direct application of the first-order optimality condition and second demonstrate that the proposed algorithm is more robust than the IRLS version w.r.t the measurement noise level. To reach these goals, this communication is divided into two parts. In section 2, the novel IR algorithm, referred to as IR$\ell_{p,q}$ algorithm in the rest of the paper, is introduced in parallel with the original IRLS algorithm, in order to better highlight the main differences between both resolution algorithms. Sec-

tion 3 is devoted to the detailed comparison of the above-mentioned algorithm through a numerical experiment, demonstrating that each algorithm exhibit a different behavior w.r.t. the measurement noise level. More specifically, the novel IR$\ell_{p,q}$ algorithm allows obtaining more consistent reconstructions for a wider range of Signal-to-Noise ratios (SNR).

2. Novel resolution algorithm - IR$\boldsymbol{\ell_{p,q}}$ algorithm

The mathematical formulation at the basis of the space-frequency multiplicative regularization implies the implementation of an iterative procedure. In our original paper, an adapted IRLS algorithm have been proposed [14]. Here, an alternative IR$\ell_{p,q}$ algorithm, based on the direct application of the first-order optimality condition, is presented. Basically, the resolution process is divided into three main steps whatever the algorithm considered:

1. Set $k = 0$ and initialize $\widehat{\mathbf{F}}^{(0)}$
2. **while** convergence is not reached
   a. Main iteration - Compute $\widehat{\mathbf{F}}^{(k+1)}$
   b. Monitor the convergence

   end while
3. **return** $\widehat{\mathbf{F}}$

In the present contribution, the initialization process as well as the convergence monitoring are not described and the interested reader can refer to Refs. [14, 18] for further information. Actually, the main difference between both algorithms lies in the main iteration when computing the force vector at iteration $k + 1$ (step 2.a).

The basic idea behind the IRLS algorithm is to define a fixed-point iteration having a unique and explicit solution, so as to recover the solution of the minimization problem given by Eq. (1) after convergence of the iterative process. To this end, the regularization term is recast into a squared weighted ℓ_2-norm regularization term. In doing so, the solution vector at iteration $k+1$ is sought as the solution of the following minimization problem:

$$\widehat{\mathbf{F}}^{(k+1)} = \underset{\mathbf{F}\setminus\{\mathbf{0}\}}{\operatorname{argmin}} \ \|\mathbf{X}-\mathbf{H}\mathbf{F}\|_2^2 \cdot \left\|\mathbf{W}^{(k+1)^{1/2}}\mathbf{F}\right\|_2^2, \tag{2}$$

where $\mathbf{W}^{(k+1)}$ is the diagonal global weighting matrix defined as a function of $\widehat{\mathbf{F}}^{(k)}$.

On the contrary, the main iteration of the IR$\ell_{p,q}$ algorithm relies on the direct application of the first-order optimality condition to the functional:

$$J(\mathbf{F}) = \|\mathbf{X}-\mathbf{H}\mathbf{F}\|_2^2 \cdot \|\mathbf{F}\|_{p,q}^q. \tag{3}$$

In other words, the solution vector at iteration $k+1$ is derived from the relation:

$$\left.\frac{\partial J(\mathbf{F})}{\partial \mathbf{F}}\right|_{\mathbf{F}=\widehat{\mathbf{F}}^{(k+1)}} = \mathbf{0}. \tag{4}$$

However, whatever the algorithm considered, the force vector at iteration $k+1$ is written:

$$\widehat{\mathbf{F}}^{(k+1)} = \left(\mathbf{H}^H\mathbf{H} + \alpha^{(k+1)}\,\mathbf{W}^{(k+1)}\right)^{-1}\mathbf{H}^H\mathbf{X}, \tag{5}$$

where the adaptive regularization parameter $\alpha^{(k+1)}$ is defined such that:

$$\alpha^{(k+1)} = \begin{cases} \dfrac{\left\| \mathbf{X} - \mathbf{H}\widehat{\mathbf{F}}^{(k)} \right\|_2^2}{\left\| \mathbf{W}^{(k+1)^{1/2}} \widehat{\mathbf{F}}^{(k)} \right\|_2^2} & \text{for IRLS} \\ \dfrac{\left\| \mathbf{X} - \mathbf{H}\widehat{\mathbf{F}}^{(k)} \right\|_2^2}{\left\| \widehat{\mathbf{F}}^{(k)} \right\|_{p,q}^q} & \text{for IR}\ell_{p,q} \end{cases}. \tag{6}$$

Regarding the global weighting matrix $\mathbf{W}^{(k+1)}$, its coefficients are expressed:

$$w_I^{(k+1)} = w_i^{s\,(k+1)} \cdot w_{ij}^{f\,(k+1)}, \tag{7}$$

where $I = j + n_f\,(i-1)$ is a global index, while $w_i^{s\,(k+1)}$ and $w_{ij}^{f\,(k+1)}$ are the weighting coefficients related to the space (superscript s) and frequency (superscript f) domains. Formally, $w_i^{s\,(k+1)}$ and $w_{ij}^{f\,(k+1)}$ are written (see Appendix A for a detailed derivation):

$$w_{ij}^{f\,(k+1)} = \left[\max\left(\epsilon_f, \left| \widehat{F}_{ij}^{(k)} \right| \right) \right]^{p-2} \tag{8}$$

and

$$w_i^{s\,(k+1)} = \begin{cases} \left[\max\left(\epsilon_s^2, \sum_{j=1}^{n_f} w_{ij}^{f\,(k+1)} \left| \widehat{F}_{ij}^{(k)} \right|^2 \right) \right]^{\frac{q}{p}-1} & \text{for IRLS} \\ \frac{q}{2} \left[\max\left(\epsilon_s^p, \sum_{j=1}^{n_f} \left| \widehat{F}_{ij}^{(k)} \right|^p \right) \right]^{\frac{q}{p}-1} & \text{for IR}\ell_{p,q} \end{cases}. \tag{9}$$

where $\widehat{F}_{ij}^{(k)}$ is the force at reconstruction point i and frequency f_j identified at iteration k[2], while ϵ_f and ϵ_s are damping parameters avoiding infinite weights when $p < 2$ and $q < p$. Practically, it has been chosen to set $\epsilon_f = \epsilon_s = \epsilon$,

[2]To perform the calculation of the weighting coefficients detailed in Appendix A, the gloabal force vector must be recast into a matrix beforehand.

whose value is calculated so that 5% of the values $\left|\widehat{\mathbf{F}}^{(0)}\right|$ are less than or equal to ϵ.

All in all, the derivation of the IRLS and IR$\ell_{p,q}$ algorithms given above clearly points out the main differences between these algorithms. More specifically, the only difference lies in the calculation of the adaptive parameter $\alpha^{(k+1)}$ and the weighting coefficient $w_i^{s\,(k+1)}$. Consequently, the implementation of the IR$\ell_{p,q}$ algorithm is straightforward, since it only requires a slight modification of the original IRLS algorithm. As a side note, it is worth noting that both algorithm are strictly identical for $p = q = 2$.

3. Numerical experiment

The present numerical experiment intends to assess the performances of both IRLS and IR$\ell_{p,q}$ algorithms w.r.t. the measurement noise level. It allows evaluating the intrinsic behavior of each algorithm by eliminating all the uncertainties related to any experimental set-up. The results of this study also make possible to investigate the applicability of the novel resolution algorithm for solving force reconstruction problems.

3.1. Problem description

The structure under consideration is a simply supported steel beam of length 1 m and cross-sectional area $1{\times}10^{-4}$ m^2. The beam is excited by a broadband unit point force from 50 Hz to 500 Hz (Frequency resolution: 1 Hz – $n_f = 451$). The point force is applied at $x_0 = 0.6$ m from the left end of the beam.

To synthesize the measured vibration field, the exact global displacement vector $\mathbf{X_{exact}}$ is first computed from a modal expansion based on the analytical modes of the beam on a set of 21 points evenly-spaced from the left to the right end of the structure ($n_m = 21$). For this calculation, a structural damping ratio of 1% has been considered. Then, a Gaussian white noise with some prescribed SNR has been added to the exact data to simulate the unavoidable errors in the measurement process. At this stage, the five first resonance frequencies of the structure are listed in Table 1 for the sake of completeness.

Table 1: Five first resonance frequencies of the beam

ID	1	2	3	4	5
Value (Hz)	23.45	93.81	211.08	375.25	586.33

Regarding now the computation of the global transfer functions matrix $\mathbf{H}$ of the structure, the finite element method has been used to avoid the so-called inverse crime [19]. Practically, it has been computed from a FE mesh made up with 20 plane beam elements, designed for perfectly matching the measurement mesh ($n_r = 21$). More specifically, a FE model of the beam with free boundary conditions has been employed, assuming that only the transverse forces acting on the structure are of primary interest. In doing so, it is possible to identify both the external and reaction forces over the beam[3]. From a mechanical perspective, this can be easily explained by

[3]Formally, it is possible to compute $\mathbf{H}$ from a FE model having the same boundary conditions. In this case, however, the reaction forces cannot be directly identified.

recalling that the system considered for the reconstruction corresponds to the beam without its supports. It results that the reaction forces stemming from the mechanical connection of the beam to its support appear as external forces in the considered reconstruction model. More specifically, the intention is to illustrate the ability of the proposed approach to reconstruct a spatially sparse excitation field composed of functionally dependent sources.

For the sake of clarity, an overview of the numerical experiment described above is proposed in Fig. 1.

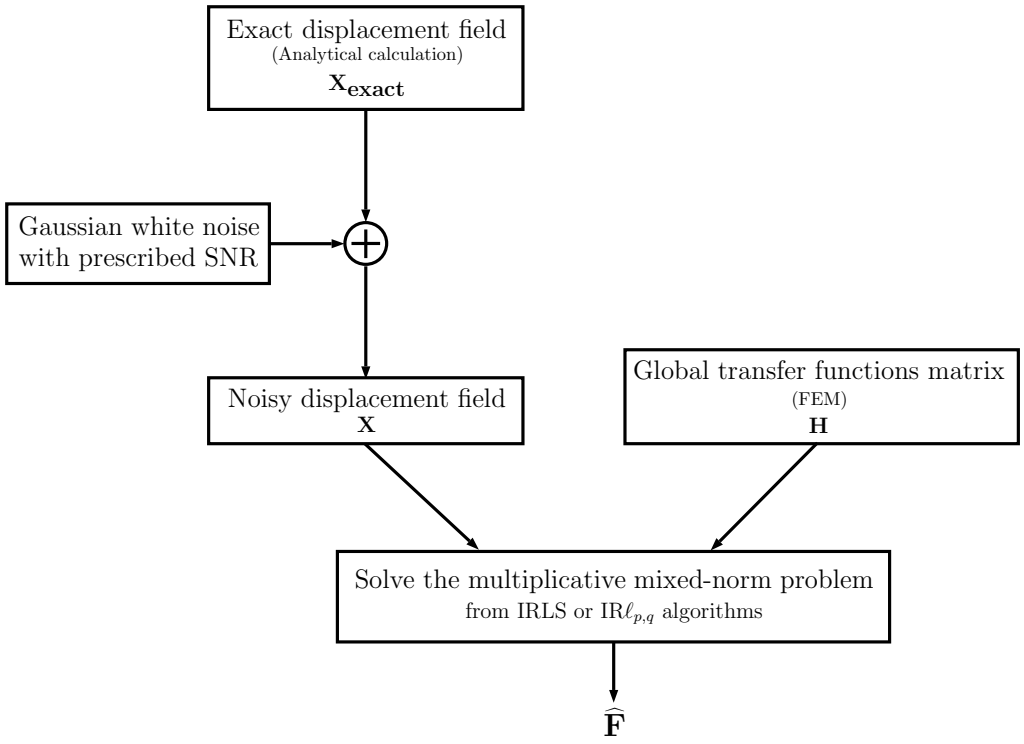

Figure 1: Overview of the numerical experiment

Finally, it is important to define the force vector, that will serve as reference for comparison, as well as the indicators, that will help us to analyze

the behavior of both algorithms in terms of computational performance and reconstruction quality.

In the present paper, the reference force vector $\mathbf{F_{ref}}$ is obtained from the following relation:

$$\mathbf{F_{ref}} = \mathbf{H}^{-1}\,\mathbf{X_{exact}}. \tag{10}$$

Fig. 2 presents the reference force vector as a space-frequency plot. As expected from the problem description, the reference excitation field is indeed spatially sparse, while the excitation signal is broadband. Regarding the def-

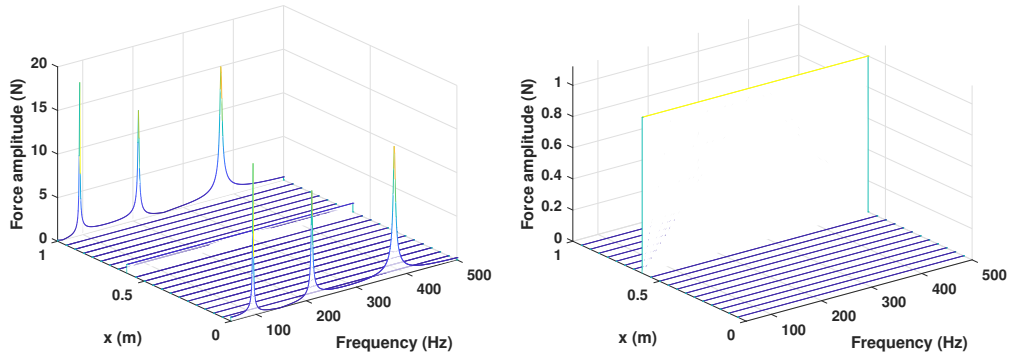

(a) (b)

Figure 2: Space-frequency plot of the reference force vector $\mathbf{F_{ref}}$ – (a) Full plot and (b) Zoomed portion of the plot excluding the reaction forces

inition of a set of indicators measuring the solution accuracy, we have chosen to implement three particular indicators: the global relative error (GRE), the relative error on the reaction forces (RERF) and the global peak error (GPE). Basically, GRE is a global indicator of the reconstruction quality and

is expressed as:

$$\mathrm{GRE} = \frac{\left\|\widehat{\mathbf{F}} - \mathbf{F}_{\mathbf{ref}}\right\|_1}{\|\mathbf{F}_{\mathbf{ref}}\|_1}. \tag{11}$$

Similarly, RERF is an indicator of the reconstruction quality of the reaction forces, defined such that:

$$\mathrm{RERF} = \frac{\left\|\widehat{\mathbf{F}}^{(\mathrm{rf})} - \mathbf{F}_{\mathbf{ref}}^{(\mathrm{rf})}\right\|_1}{\left\|\mathbf{F}_{\mathbf{ref}}^{(\mathrm{rf})}\right\|_1}, \tag{12}$$

where $\widehat{\mathbf{F}}^{(\mathrm{rf})}$ is the force vector of the identified reaction forces, while $\mathbf{F}_{\mathbf{ref}}^{(\mathrm{rf})}$ is the corresponding reference force vector.

Finally, GPE is an indicator defining the reconstruction quality of the point force spectrum. This indicator is mathematically written:

$$\mathrm{GPE} = \frac{\left\|\widehat{\mathbf{F}}^{(\mathrm{pf})} - \mathbf{F}_{\mathbf{ref}}^{(\mathrm{pf})}\right\|_1}{\left\|\mathbf{F}_{\mathbf{ref}}^{(\mathrm{pf})}\right\|_1}, \tag{13}$$

where $\widehat{\mathbf{F}}^{(\mathrm{pf})}$ is the point force spectrum identified at point x_0, while $\mathbf{F}_{\mathbf{ref}}^{(\mathrm{pf})}$ is the corresponding reference point force spectrum.

3.2. Application

In this section, the overall reconstruction performances of both IRLS and IR$\ell_{p,q}$ algorithms are analyzed and compared. Before that, it remains to define the tuning parameters (p, q) to be able to apply the space-frequency regularization. To this end, one has to exploit one's prior knowledge of the sources to identify. From the description of the test and the analysis of Fig. 2, one has to identify a broadband sparse excitation. Practically, this observation leads us to promote the spatial sparsity of the solution and the

continuity of its spectral content. Hence, following the recommendations given in the introduction of this paper and our previous work on this topic [14], one chooses to set $(p, q) = (2, 0.5)$ for the rest of the paper.

3.3. IRLS algorithm

To have a fair point of comparison, the space-frequency regularization is first solved from the IRLS algorithm for three different measurement noise levels, namely SNR $= 35, 25, 15$ dB. The corresponding results are presented in Fig. 3 and Table 2. Several comments can be made. First of all, very good reconstructions are obtained for high SNR values. For moderate SNR values, the results are more contrasted, since the reaction forces are satisfyingly identified, as well as the point force location. However, the point force amplitude is globally underestimated, since the identified amplitude tends to decrease with frequency. Finally, for low SNR values, the IRLS algorithm diverges and no solution is obtained.

Table 2: Performances of the IRLS algorithm with respect to the measurement noise level corrupting the data – N_{it}: Number of iterations of the algorithm

SNR (dB)	GRE (%)	RERF (%)	GPE (%)	N_{it}
35	2.1	1.5	3.6	19
25	13.8	7.6	27.7	27
15	–	–	–	–

3.4. IR$\ell_{p,q}$ algorithm

Contrary to what has been observed in the previous section, more consistent reconstructions are obtained from the IR$\ell_{p,q}$ algorithm as shown by the

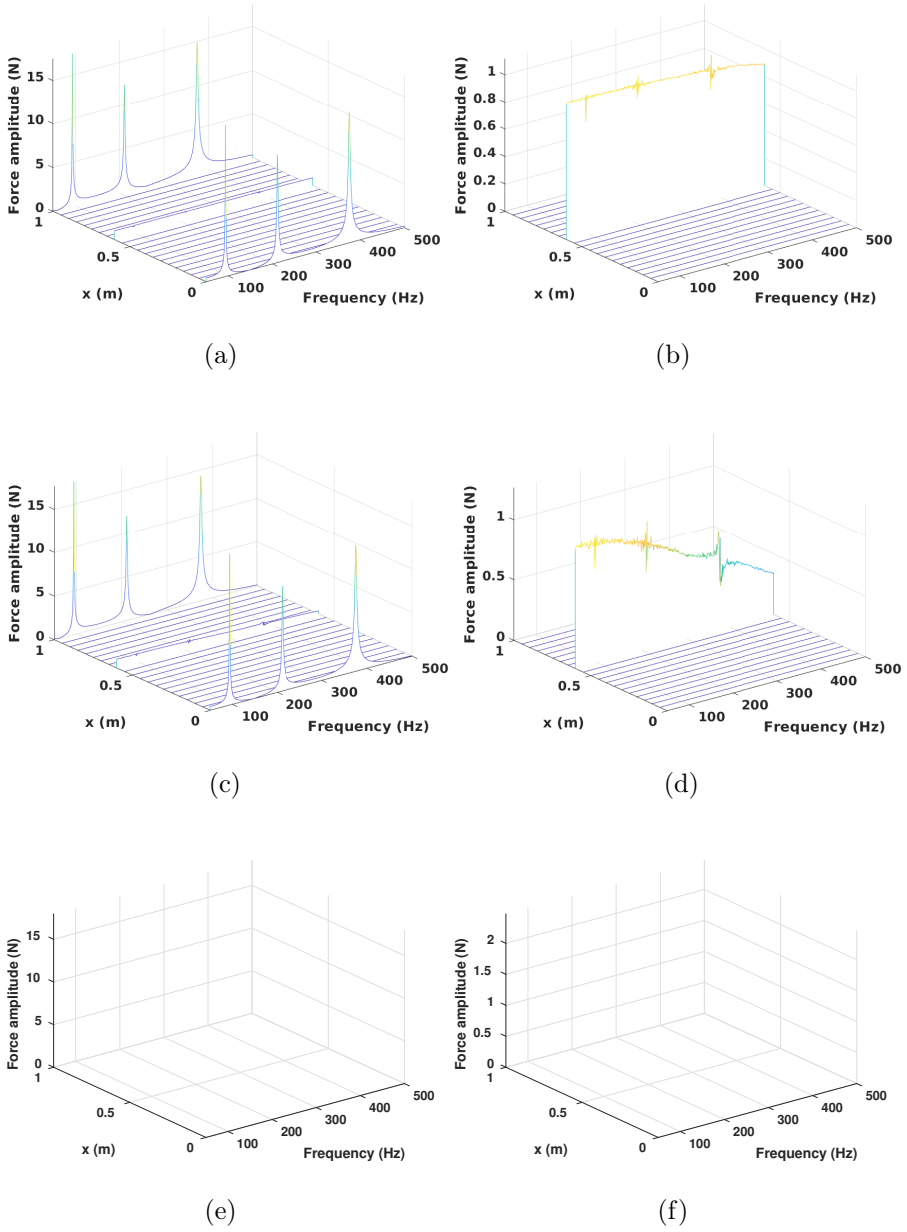

Figure 3: Space-frequency plot of the force vector $\widehat{\mathbf{F}}$ identified from the IRLS algorithm – Left column: Full plot, Right column: Zoomed portion – (a) and (b) SNR = 35 dB, (c) and (d) SNR = 25 dB, (e) and (f) SNR = 15 dB

results given in Fig. 4 and Table 3. Indeed, consistent reconstructions are obtained for high and moderate SNR values, even if some discrepancies can be observed around the resonance frequencies. For low SNR values, the proposed algorithm does not diverge anymore, since a solution can be computed. However, the quality of the reconstructed solution is not as good as excepted, but a careful analysis of the results allows obtaining useful information. In particular, it should be noted that the reaction forces and the point force location are rather well identified, while the point force amplitude is largely underestimated and decreases with the frequency.

Table 3: Performances of the IR$\ell_{p,q}$ algorithm with respect to the measurement noise level corrupting the data – N_{it}: Number of iterations of the algorithm

SNR (dB)	GRE (%)	RERF (%)	GPE (%)	N_{it}
35	1.2	1.0	1.6	21
25	4.9	3.1	8.9	20
15	25.0	14.3	48.8	26

3.5. Summary

The two previous sections allows demonstrating that the proposed IR$\ell_{p,q}$ algorithm exhibits a better robustness with respect to the measurement noise level than its IRLS counterpart. More specifically, the GRE, RERF and GPE indicators allows confirming the qualitative conclusion drawn from the visual inspection of Figs. 3 and 4. They indeed show that reconstruction errors are consistently less for the IR$\ell_{p,q}$ algorithm than for the IRLS algorithm. Unfortunately, this observation is not supported by any theoretical argument.

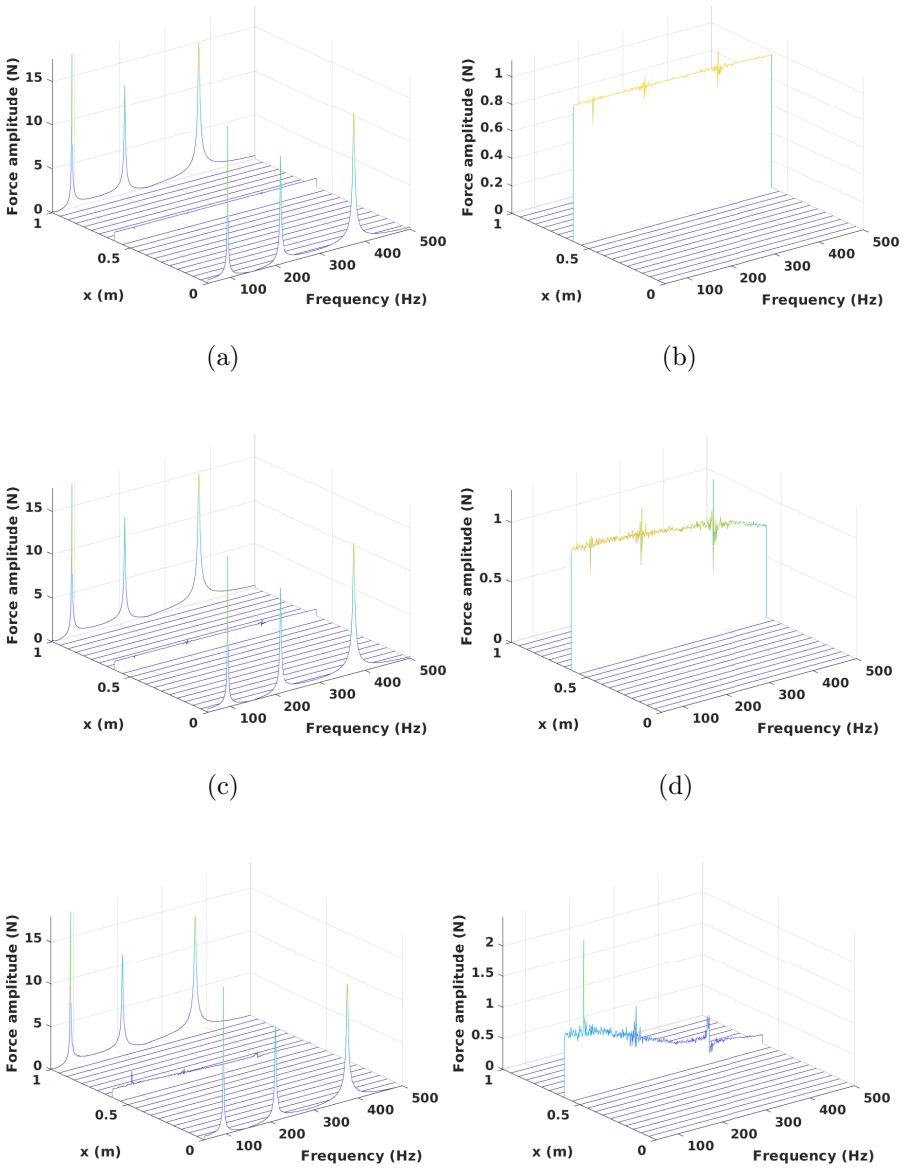

Figure 4: Space-frequency plot of the force vector $\widehat{\mathbf{F}}$ identified from the IR$\ell_{p,q}$ algorithm – Left column: Full plot, Right column: Zoomed portion – (a) and (b) SNR = 35 dB, (c) and (d) SNR = 25 dB, (e) and (f) SNR = 15 dB

Indeed, finding a mathematical proof of convergence for the proposed algorithms is far from easy task and remains an open issue, especially because the value of the regularization parameter changes at each iteration. It results that proving mathematically that the IR$\ell_{p,q}$ converges to a better solution than that obtained from the IRLS algorithm is all the more difficult.

It is, however, possible to explain why the algorithms leads to different solutions. To this end, it is interesting to analyze the convergence path of both algorithms by analyzing the evolution of the adaptive regularization parameter and the condition number throughout the iterations. The results presented in Fig. 5 show that the IRLS and IR$\ell_{p,q}$ have different dynamics, even if both algorithms share some similarities in the definition of the weighting coefficients. In particular, this highlights the central role of the adaptive regularization parameter in the trajectory of the convergence path and the resulting solutions.

To get further insights into the algorithms behavior, it is interesting to study the existence of local minimizers for the proposed multiplicative mixed-norm regularization. As shown in Ref. [18], the multiplicative functional has, at least, three minimizers: (i) the least-squares solution when $\widehat{\alpha} = \alpha_1 \to 0$, (ii) the zero vector when $\widehat{\alpha} = \alpha_2 \to +\infty$ and (iii) a local minimizer when $\widehat{\alpha} \in [\alpha_1, \alpha_2]$ ($\widehat{\alpha}$: value of the adaptive regularization parameter at convergence). Because the convergence paths of the IRLS and IR$\ell_{p,q}$ algorithms are different and result in different reconstructed excitation fields, this suggests that the existence of a local minimizer is not necessarily guaranteed especially for very noisy measurement data. To formalize a finding method, one has to note that

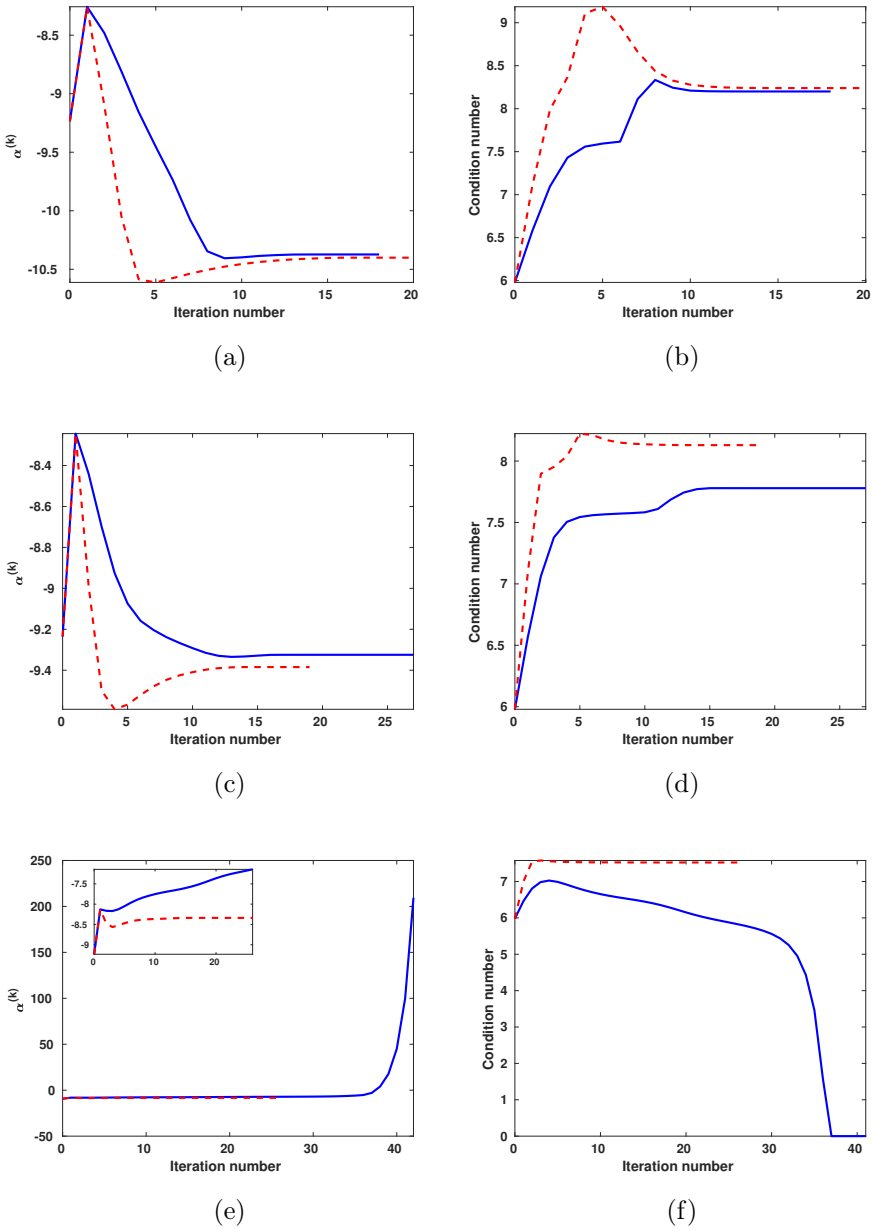

Figure 5: Evolution of the adaptive regularization parameter and condition number throughout the iterations – Left column: adaptive regularization parameter, Right column: condition number – (a) and (b) SNR = 35 dB, (c) and (d) SNR = 25 dB, (e) and (f) SNR = 15 dB – (—) IRLS algorithm and (– –) IR$\ell_{p,q}$ algorithm (the ordinate are scaled logarithmically using the common logarithm).

Eqs. (5) and (6) imply that [20]:

$$\frac{\widehat{\alpha}\left\|\widehat{\mathbf{W}}^{1/2}\widehat{\mathbf{F}}\right\|_2^2}{\left\|\mathbf{X}-\mathbf{H}\widehat{\mathbf{F}}\right\|_2^2} \approx 1 \tag{14}$$

for the IRLS algorithm and:

$$\frac{\widehat{\alpha}\left\|\widehat{\mathbf{F}}\right\|_{p,q}^q}{\left\|\mathbf{X}-\mathbf{H}\widehat{\mathbf{F}}\right\|_2^2} \approx 1 \tag{15}$$

for the IR$\ell_{p,q}$ algorithm. In previous equations, $\widehat{\mathbf{W}}$ and $\widehat{\mathbf{F}}$ are, respectively, the weighting matrix and the force vector obtained at convergence of the considered algorithm. The previous observation suggests the definition of an indicator that allows determining the existence of local minimizers. Formally, this indicator is written for any α:

$$\phi(\alpha) = \begin{cases} \dfrac{\alpha\left\|\widehat{\mathbf{W}}_\alpha^{1/2}\widehat{\mathbf{F}}_\alpha\right\|_2^2}{\left\|\mathbf{X}-\mathbf{H}\widehat{\mathbf{F}}_\alpha\right\|_2^2} & \text{for IRLS} \\ \dfrac{\alpha\left\|\widehat{\mathbf{F}}_\alpha\right\|_{p,q}^q}{\left\|\mathbf{X}-\mathbf{H}\widehat{\mathbf{F}}_\alpha\right\|_2^2} & \text{for IR}\ell_{p,q} \end{cases}, \tag{16}$$

where $\widehat{\mathbf{W}}_\alpha$ and $\widehat{\mathbf{F}}_\alpha$ are, respectively, the weighting matrix and the force vector obtained at convergence of the considered algorithm for a fixed given α[4]. It results from the previous definition that a minimizer (local or global) is found when $\phi(\alpha) = 1$.

[4] $\widehat{\mathbf{F}}_\alpha$ is obtained by solving Eq. (5) by fixing the adaptive regularization parameter to a constant value α for all the iterations until convergence of the IRLS and IR$\ell_{p,q}$ algorithms.

The plots of $\phi(\alpha)$ obtained from the IRLS and IR$\ell_{p,q}$ algorithms for SNR = 35, 25, 15 dB are presented in Fig. 6. This figure shows that the application of the IR$\ell_{p,q}$ algorithm leads to only three minimizers whatever the SNR considered. More specifically, the solution associated to the smallest α corresponds to the least-squares solution, the solution associated to the largest α is the zero vector, while the last one is the solution obtained for $\widehat{\alpha}$ computed from Eq. (6) (indicated by the marker $*$ in Fig. 6). On the contrary, the IRLS algorithm behaves rather differently. Indeed, its application for high and moderate SNR leads to five minimizers. Actually, only the second one, corresponding to the solution obtained for $\widehat{\alpha}$, leads to a consistent solution, since the first minimizer corresponds to the least-squares solution, while the last three correspond to the zero vector. Unfortunately, in case of low SNR, the IRLS algorithm leads to only one minimizer associated to the least-squares solution. It should be emphasized here that both algorithms converge to a value of $\widehat{\alpha}$ greater than that used to initialize the iterations. In any case, the initial value is greater than that leading to the least-squares solution, which explains why the IRLS algorithm diverges for low SNR.

Another interesting observation is related to the low-pass effect of the algorithms on the reconstruction of the forces spectra observed and commented in the previous sections (see Figs. 3 and 4)[5]. Actually, we are prone to think that this effect is somewhat related to the behavior of Tikhonov-like regularizations that lead to the definition of the so-called filter factors

[5]It should be be mentioned that this problem has not been observed experimentally (see Ref. [14])

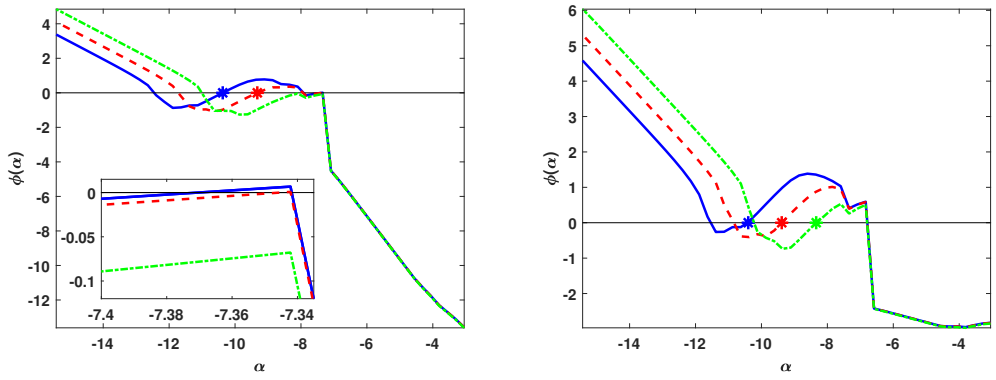

(a) (b)

Figure 6: Plots of $\phi(\alpha)$ for (a) the IRLS algorithm and (b) the IR$\ell_{p,q}$ algorithm – (—) SNR = 35 dB, (– –) SNR = 25 dB, (– · –) SNR = 15 dB and ($*$) $\phi(\widehat{\alpha})$ (the abscissa and the ordinate are scaled logarithmically using the common logarithm)

[21, 22], that damp or filter the singular values much smaller than the regularization parameter. In this regard, one can infer that the singular values associated to the higher frequencies of the system are the most affected by this filtering effect. This is probably an immediate consequence of the definition of a unique regularization parameter induced by the formulation. Two potential alternative can be imagined to compensate this effect. The first one consists in defining one regularization parameter per frequency or group of frequencies. Such an approach does not involve a mixed-norm regularization term anymore and could be directly solved using the extended multiplicative regularization proposed by the authors in Ref. [17]. The second possibility consists in slightly modifying the regularization term as proposed by Regińska or Viloche Bazán et al. in Refs. [23, 24]. However, their applicability to the present problem is left for future works.

Finally, even if the comparison of the space-frequency and the ordinary multiplicative regularizations is outside the scope of this paper, the results obtained from the ordinary multiplicative regularization, which solves the inverse problem frequency by frequency, are given in Appendix B for the sake of completeness. In this appendix, interested readers will find useful information regarding the application of both regularization strategies in a similar context, as partially done in Ref. [14].

4. Conclusion

This short communication can be viewed as an extension to our previous work on the space-frequency multiplicative regularization, since it introduces a novel iterative algorithm, called IR$\ell_{p,q}$, to solve mixed-norm regularization problems. As pointed out by the numerical experiment we carried out, the proposed IR$\ell_{p,q}$ offers a better robustness than the original IRLS algorithm w.r.t. the measurement noise level. This contribution also shows that the resolution algorithm is the key for a successful force reconstruction and suggests that the research efforts must be continued. Finally, it is worth noting that, even if the IR$\ell_{p,q}$ algorithm has been derived and applied in the context of force reconstruction, it is actually very general, since it can directly be applied to the wider class of linear inverse problems.

Appendix A. Calculation of the weighting matrix W

The purpose of this appendix is to detail the calculation of the weighting coefficients w_{ij}^f and w_i^s given in Eqs. (8) and (9) for both IRLS and IR$\ell_{p,q}$ algorithms.

To establish the mathematical expression of the weighting coefficients for IRLS and IR$\ell_{p,q}$ algorithms, one has to remind that the mixed $\ell_{p,q}$-norm is a matrix norm. In other words, the global force vector $\mathbf{F}$ must be recast into a matrix, whose coefficient $F_{ij} = F_i(f_j)$ is the force at reconstruction point i and frequency f_j, to perform the derivation of the weighting coefficients. It results that the regularization term of the space-frequency multiplicative regularization is explicitly written:

$$\|\mathbf{F}\|_{p,q}^{q} = \sum_{i=1}^{n_r} \left(\sum_{j=1}^{n_f} |F_{ij}|^{p} \right)^{\frac{q}{p}}. \tag{A.1}$$

Appendix A.1. IRLS algorithm

The basic idea of the IRLS algorithm consists in recasting the mixed $\ell_{p,q}-$norm to the power of q into a squared weighted ℓ_2-norm. From this definition, the weighting coefficients w_{ij}^{f} and w_i^{s} are determined as follows:

$$\begin{aligned}
\|\mathbf{F}\|_{p,q}^{q} &= \sum_{i=1}^{n_r} \left(\sum_{j=1}^{n_f} |F_{ij}|^{p} \right)^{\frac{q}{p}} \\
&= \sum_{i=1}^{n_r} \left(\sum_{j=1}^{n_f} |F_{ij}|^{p-2} |F_{ij}|^{2} \right)^{\frac{q}{p}} \\
&= \sum_{i=1}^{n_r} \left(\sum_{j=1}^{n_f} w_{ij}^{f} |F_{ij}|^{2} \right)^{\frac{q}{p}} \\
&= \sum_{i=1}^{n_r} \left[\left(\sum_{j=1}^{n_f} w_{ij}^{f} |F_{ij}|^{2} \right)^{\frac{q}{p}-1} \cdot \sum_{j=1}^{n_f} w_{ij}^{f} |F_{ij}|^{2} \right] \\
&= \sum_{i=1}^{n_r} \sum_{j=1}^{n_f} w_i^{s} \, w_{ij}^{f} |F_{ij}|^{2} = \left\| \mathbf{W}^{1/2} \mathbf{F} \right\|_2^2 .
\end{aligned} \tag{A.2}$$

The previous equation clearly shows that the weighting coefficients w_{ij}^{f}

and w_i^s are theoretically defined by:

$$w_{ij}^f = |F_{ij}|^{p-2} \quad \text{and} \quad w_i^s = \left(\sum_{j=1}^{n_f} w_{ij}^f \, |F_{ij}|^2 \right)^{\frac{q}{p}-1}. \tag{A.3}$$

However, to avoid infinite weights when $p < 2$ and $q < p$, two damping parameters, ϵ_f and ϵ_s, must be introduced so that:

$$w_{ij}^f = \left[\max \left(\epsilon_f, |F_{ij}| \right) \right]^{p-2} \quad \text{and} \quad w_i^s = \left[\max \left(\epsilon_s^2, \sum_{j=1}^{n_f} w_{ij}^f \, |F_{ij}|^2 \right) \right]^{\frac{q}{p}-1} \tag{A.4}$$

Finally, Eq. (A.2) allows also demonstrating that the coefficients of the global weighting matrix $\mathbf{W}$ are written:

$$w_I = w_i^s \cdot w_{ij}^f, \tag{A.5}$$

where $I = j + n_f \, (i-1)$.

Appendix A.2. IR$\ell_{p,q}$ algorithm

For the IR$\ell_{p,q}$ algorithm, the weighting coefficients w_{ij}^f and w_i^s result from the direct application of the first-order optimality condition to the functional:

$$J(\mathbf{F}) = \|\mathbf{X} - \mathbf{H}\mathbf{F}\|_2^2 \cdot \|\mathbf{F}\|_{p,q}^q. \tag{A.6}$$

By definition, the first-order optimality condition consists in taking the gradient of the functional $J(\mathbf{F})$ w.r.t. $\mathbf{F}$ and setting the gradient to zero [see Eq. (4)]. In doing so, one finds:

$$2 \left(\mathbf{H}^H \mathbf{H} - \mathbf{H}^H \mathbf{X} \right) \cdot \|\mathbf{F}\|_{p,q}^q + 2 \, \|\mathbf{X} - \mathbf{H}\mathbf{F}\|_2^2 \cdot \left(\frac{1}{2} \frac{\partial \|\mathbf{F}\|_{p,q}^q}{\partial \mathbf{F}} \right) = \mathbf{0}. \tag{A.7}$$

Consequently, the desired weighting coefficients are obtained by calculating $\frac{1}{2}\frac{\partial \|\mathbf{F}\|_{p,q}^q}{\partial \mathbf{F}}$. To render this derivation more straightforward, let us carry out this calculation component-wise, namely:

$$\begin{aligned}
\frac{1}{2}\frac{\partial \|\mathbf{F}\|_{p,q}^q}{\partial F_{ij}} &= \frac{1}{2}\sum_{k=1}^{n_r} \frac{\partial \left(\sum_{l=1}^{n_f} |F_{kl}|^p\right)^{\frac{q}{p}}}{\partial F_{ij}} \\
&= \sum_{i=1}^{n_r} \frac{q}{2p}\left(\sum_{l=1}^{n_f} |F_{kl}|^p\right)^{\frac{q}{p}-1} \cdot \frac{\partial \sum_{j=1}^{n_f} |F_{kl}|^p}{\partial F_{ij}} \\
&= \sum_{k=1}^{n_r}\sum_{l=1}^{n_f} \frac{q}{2}\left(\sum_{l=1}^{n_f} |F_{kl}|^p\right)^{\frac{q}{p}-1} |F_{kl}|^{p-2} F_{kl}\, \delta_{ik}\, \delta_{jl} \\
&= \frac{q}{2}\left(\sum_{j=1}^{n_f} |F_{ij}|^p\right)^{\frac{q}{p}-1} |F_{ij}|^{p-2}\, F_{ij} \\
&= w_i^s\, w_{ij}^f\, F_{ij}.
\end{aligned} \tag{A.8}$$

The previous equation clearly shows that the weighting coefficients w_{ij}^f and w_i^s are theoretically defined by:

$$w_{ij}^f = |F_{ij}|^{p-2} \quad \text{and} \quad w_i^s = \frac{q}{2}\left(\sum_{j=1}^{n_f} |F_{ij}|^p\right)^{\frac{q}{p}-1}. \tag{A.9}$$

As for the IRLS version, two damping parameters, ϵ_f and ϵ_s , must be introduced to avoid infinite weights when $p < 2$ and $q < p$. In doing so, the definition of the weighting coefficients w_{ij}^f and w_i^s becomes:

$$w_{ij}^f = \left[\max\left(\epsilon_f, |F_{ij}|\right)\right]^{p-2} \quad \text{and} \quad w_i^s = \frac{q}{2}\left[\max\left(\epsilon_s^p, \sum_{j=1}^{n_f} |F_{ij}|^p\right)\right]^{\frac{q}{p}-1}. \tag{A.10}$$

As a side note, it is worth noting that, in matrix notation, Eq. (A.8) is expressed as:

$$\frac{1}{2}\frac{\partial \|\mathbf{F}\|_{p,q}^q}{\partial \mathbf{F}} = \mathbf{W}\mathbf{F}, \tag{A.11}$$

where $\mathbf{W}$ is a diagonal matrix and $\mathbf{F}$ is here expressed as a column vector.

The latter relation implies that Eq. (A.7) is written:

$$2\left(\mathbf{H}^H\mathbf{H}-\mathbf{H}^H\mathbf{X}\right)\cdot\|\mathbf{F}\|_{p,q}^{q}+2\,\|\mathbf{X}-\mathbf{H}\mathbf{F}\|_2^2\cdot\mathbf{W}\mathbf{F}=\mathbf{0}. \tag{A.12}$$

The previous relation allows obtaining the expression of the global force vector at iteration $k+1$ of the IR$\ell_{p,q}$ algorithm, that is:

$$\widehat{\mathbf{F}}^{(k+1)}=\left(\mathbf{H}^H\mathbf{H}+\alpha^{(k+1)}\,\mathbf{W}^{(k+1)}\right)^{-1}\mathbf{H}^H\mathbf{X}, \tag{A.13}$$

where the adaptive regularization parameter $\alpha^{(k+1)}$ is defined such that:

$$\alpha^{(k+1)}=\frac{\left\|\mathbf{X}-\mathbf{H}\widehat{\mathbf{F}}^{(k)}\right\|_2^2}{\left\|\widehat{\mathbf{F}}^{(k)}\right\|_{p,q}^{q}}. \tag{A.14}$$

Appendix B. Comparison with the ordinary multiplicative regularization

This appendix aims at providing some reconstruction results obtained from the application of the ordinary multiplicative regularization (OMR), that solves the inverse problem frequency by frequency. Basically, the formulation of the identification problem at frequency f_j is given by:

$$\widehat{\mathbf{F}}(f_j)=\underset{\mathbf{F}(f_j)\setminus\{\mathbf{0}\}}{\operatorname{argmin}}\ \|\mathbf{X}(f_j)-\mathbf{H}(f_j)\,\mathbf{F}(f_j)\|_2^2\cdot\|\mathbf{F}(f_j)\|_q^q\,, \tag{B.1}$$

where $\mathbf{H}(f_j)$, $\mathbf{X}(f_j)$ and $\mathbf{F}(f_j)$ are, respectively, the transfer functions matrix, the measured vibration field and the excitation vector at frequency f_j.

Practically, the previous formulation is solved from an IRℓ_q algorithm, whose description can be found in Ref. [17]. As done in section 3.2, the reconstruction problem is solved for three SNR values, namely 35 dB, 25 dB and 15 dB. The results presented in Fig. B.7 and Table B.4 shows that, for high and moderate SNR values, the space-frequency multiplicative regularization, solved from the IR$\ell_{p,q}$ algorithm, performs better than the ordinary multiplicative regularization, which exhibits reconstructions artifacts around the resonance frequencies of the beam. On the contrary, for low SNR values, the ordinary multiplicative regularization allows obtaining a better reconstruction of the point force spectrum outside the resonance frequencies. However, reconstruction artifacts are still observed around the resonance frequencies, while the reconstructed excitation field computed by the space-frequency multiplicative regularization is cleaner. This last observation highlights the practical interest in exploiting prior information on the excitation signals to identify.

Table B.4: Performances of the IRℓ_q algorithm (OMR) with respect to the measurement noise level corrupting the data – N_{it}: Number of iterations of the algorithm

SNR (dB)	GRE (%)	RERF (%)	GPE (%)
35	5.4	1.4	3.3
25	10.7	2.5	9.6
15	29.7	8.4	29.3

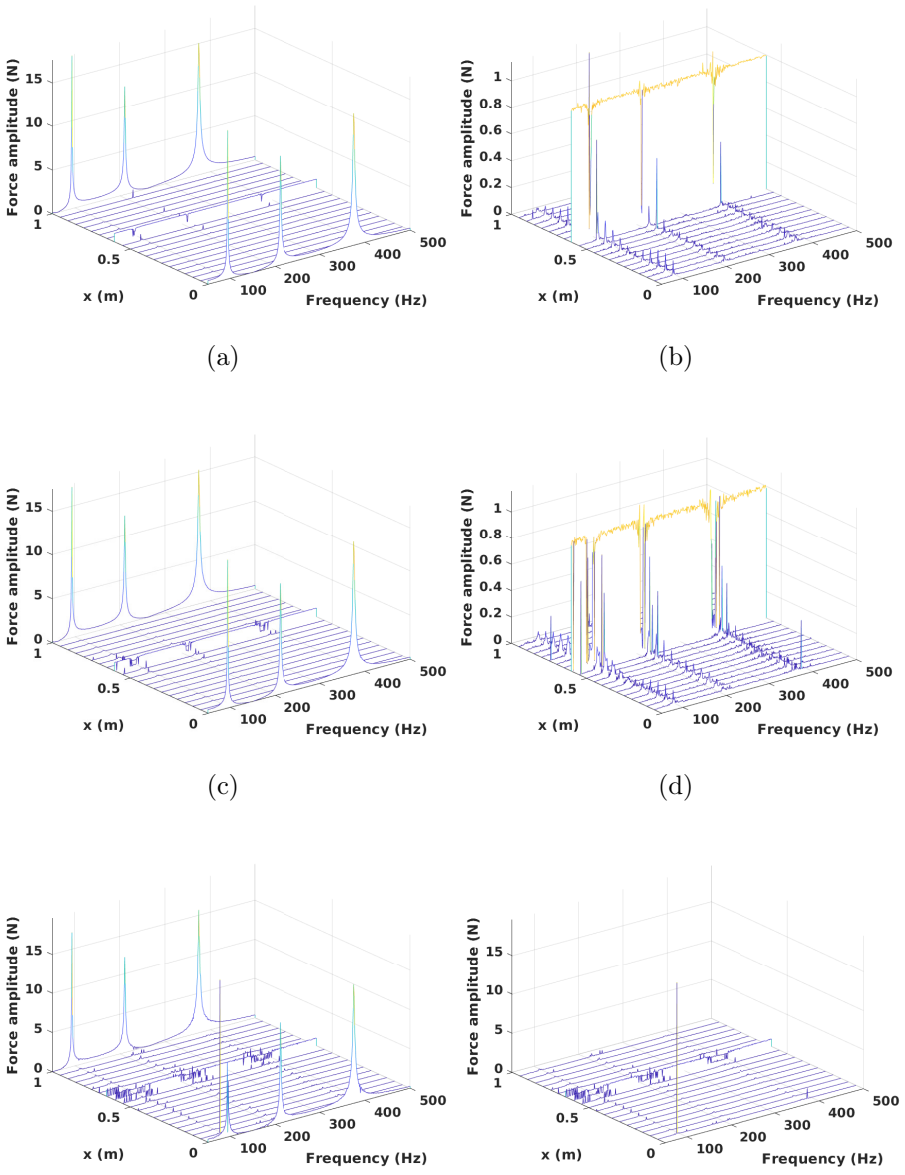

Figure B.7: Space-frequency plot of the force vector $\widehat{\mathbf{F}}$ identified from the IRℓ_q algorithm (OMR) – Left column: Full plot, Right column: Zoomed portion – (a) and (b) SNR = 35 dB, (c) and (d) SNR = 25 dB, (e) and (f) SNR = 15 dB

References

[1] S. F. Cotter, B. D. Rao, K. Engan, and K. Kreutz-Delgado. Sparse solutions to linear inverse problemswith multiple measurement vectors. *IEEE Transactions on Signal Processing*, 53 (7):2477–2488, 2005.

[2] G. Teschke and R. Ramlau. An iterative algorithm for nonlinear inverse problems with joint sparsity constraints in vector-valued regimes and an application to color impage impainting. *Inverse Problems*, 23:1851–1870, 2007.

[3] M. Fornassier and H. Rauhut. Recovery algorithm for vector-valued data with joint sparsity constraints. *SIAM Journal on Numerical Analysis*, 46 (2):577–613, 2008.

[4] M. Kowalski. Sparse regression using mixed norms. *Applied and Computational Harmonic Analysis*, 27:303–324, 2009.

[5] A. Rakotomamonjy. Surveying and comparing simultaneous sparse approximation (or group-lasso) algorithms. *Signal Porcessing*, 91 (7):1505–1526, 2011.

[6] A. Gramfort, M. Kowalski, and M. Hamalainen. Mixed-norm estimates for the m/eeg inverse problem using accelerated gradient methods. *Physics in Medecine and Biology*, 57:1937–1961, 2012.

[7] C. Zheng, G. Li, Y. Liu, and X. Wang. Subspace weighted $\ell_{2,1}$ minimization for sparse signal recovery. *EURASIP Journal on Advances in Signal Processing 2012*, 2012:98, 2012.

[8] Y. Wang, J. Wang, and Z. Xu. On recovery of block-sparse signals via mixed ℓ_2/ℓ_q $(0 < q \leq 1)$ norm minimization. *EURASIP Journal on Advances in Signal Processing 2013*, 2013:76, 2013.

[9] J Zheng, K. Lou, X. Yang, C. Bai, and J. Tang. Weighted mixed-norm regularized regression for robust face identification. *IEEE Transactions on Neural Networks and Learning Systems*, 30 (12):3788–3802, 2019.

[10] A. Rezayat, V. Nassiri, B. De Pauw, J. Ertveldt, S. Vanlanduit, and P. Guillaume. Identification of dynamic forces using group-sparsity in frequency domain. *Mechanical Systems and Signal Processing*, 70-71:756–768, 2016.

[11] A. Rezayat, V. Nassiri, S. Vanlanduit, and P. Guillaume. Force identification using mixed and penalized optimization techniques. In *Proceedings of ISMA 2014*, Leuven, Belgium, 2014.

[12] J. Wambacq, K. Maes, A. Rezayat, P. Guillaume, and G. Lombaert. Localization of dynamic forces on structures with an interior point method using group sparsity. *Mecahnical Systems and Signal Processing*, 115:593–606, 2019.

[13] B. Qiao, Zhu Mao, J. Liu, Z. Zhao, and X. Chen. Group sparse regularization for impact force identification in time domain. *Journal of Sound and Vibration*, 445:44–63, 2019.

[14] M. Aucejo and O. De Smet. A space-frequency multiplicative regularization for force reconstruction problems. *Mechanical Systems and Signal Processing*, 2018.

[15] P. Rodriguez and B. Wohlberg. An Iteratively Weighted Norm Algorithm for Total Variation Regularization. In *Proceedings of the 2006 Asilomar Conference on Signals, Systems, and Computers*, Pacific Grove, USA, 2006.

[16] B. Wohlberg and P. Rodriguez. An Iteratively Reweighted Norm Algorithm for Minimization of Total Variation Functionals. *Signal Processing, IEEE*, 14 (12):958–951, 2007.

[17] M. Aucejo and O. De Smet. Multi-parameter multiplicative regularization: An application to force reconstruction problems. *Journal of Sound and Vibration*, 469:115135 – 15 pages, 2020.

[18] M. Aucejo and O. De Smet. A multiplicative regularization for force reconstruction. *Mechanical Systems and Signal Processing*, 85:730–745, 2017.

[19] D. Colton and R. Kress. *Inverse Acoustic and Electromagnetic Scattering Theory*. Springer, Berlin, 1992.

[20] J. A. Orozco Rodriguez. *Regularization for inverse problems*. PhD thesis, University of Minnesota, 2011.

[21] P. C. Hansen. *Discrete Inverse Problems: Insight and Algorithms*. SIAM, Philadelphia, 2010.

[22] P.-A. Gauthier, A. Gérard, C. Camier, and A. Berry. Acoustical inverse problems regularization: Direct definition of filter factors using signal-to-noise ratio. *Journal of Sound and Vibration*, 333:761–773, 2014.

[23] T. Regińska. A regularization parameter in discrete ill-posed problems. *SIAM Journal on Scientfic Computing*, 17 (3):740–749, 1996.

[24] F. Viloche Bazán, L. S. Borges, and J. B. Francisco. On a generalization of regińska's parameter choice rule and its numerical realization in large-scale multi-parameter tikhonov regularization. *Applied Mathematics and Compuation*, 219:2100–2113, 2012.